Hindawi Publishing Corporation
Advances in Optical Technologies
Volume 2012, Article ID 316045, 10 pages
doi:10.1155/2012/316045

Research Article

Carrier Formation Dynamics of Organic Photovoltaics as Investigated by Time-Resolved Spectroscopy

Kouhei Yonezawa,[1] Minato Ito,[1] Hayato Kamioka,[1,2] Takeshi Yasuda,[3] Liyuan Han,[3] and Yutaka Moritomo[1,2]

[1] *Graduate School of Pure and Applied Science, University of Tsukuba, Tsukuba 305-8571, Japan*
[2] *Tsukuba Research Center for Interdisciplinary Materials Science (TIMS), University of Tsukuba, Tsukuba 305-8571, Japan*
[3] *Photovoltaic Materials Unit, National Institute for Materials Science (NIMS), Tsukuba 305-0047, Japan*

Correspondence should be addressed to Yutaka Moritomo, moritomo@sakura.cc.tsukuba.ac.jp

Received 9 April 2012; Accepted 17 May 2012

Academic Editor: Saulius Juodkazis

Bulk heterojunction (BHJ) based on a donor (D) polymer and an acceptor (A) fullerene derivative is a promising organic photovoltaics (OPV). In order to improve the incident photon-to-current efficiency (IPCE) of the BHJ solar cell, a comprehensive understanding of the ultrafast dynamics of excited species, such as singlet exciton (D^*), interfacial charge-transfer (CT) state, and carrier (D^+), is indispensable. Here, we performed femtosecond time-resolved spectroscopy of two prototypical BHJ blend films: poly(3-hexylthiophene) (P3HT)/[6,6]-phenyl C_{61}-butyric acid methyl ester (PCBM) blend film and poly(9,9′-dioctylfluorene-co-bithiophene) (F8T2)/[6,6]-phenyl C_{71}-butyric acid methyl ester ($PC_{70}BM$) blend film. We decomposed differential absorption spectra into fast, slow, and constant components via two-exponential fitting at respective probe photon energies. The decomposition procedure clearly distinguished photoinduced absorptions (PIAs) due to D^*, CT, and D^+. Based on these assignments, we will compare the charge dynamics between the F8T2/$PC_{70}BM$ and P3HT/PCBM blend films.

1. Introduction

Organic photovoltaics (OPV) is an environmentally friendly and low-cost technology, which converts the solar energy into electric one. The incident photon-to-current efficiency (IPCE) of the bulk heterojunction (BHJ) solar cell [1, 2] is governed by the three processes: (1) charge formation process at the donor (D)-acceptor (A) interface, (2) charge transport process within the organic semiconductor, and (3) charge collecting process on the Al and indium tin oxide (ITO) electrodes. The femtosecond time-resolved spectroscopy is one of the powerful tool to reveal the (1) charge formation dynamics, because we can trace the ultrafast dynamics of excited species, such as singlet exciton (D^*), interfacial charge-transfer (CT) state, and carrier (D^+) [3–5]. The photoirradiation of the D polymer (A molecule) excites an electron from the highest occupied molecular orbital (HOMO) to the lowest unoccupied molecular orbital (LUMO). We call such a photoexcited D (A) state as excitons D^* (A^*). The D^* (A^*) state migrates within the D domain (or A domain) to reach the D-A interface. At the interface, the charge transfer between D and A produces an intermediate state (CT state). The CT state consists of electrostatically bound charge pairs, where the hole is primarily localized on the D HOMO and the electron on the A LUMO. Finally, the charge separation takes place to produce free carriers D^+ (A^-).

Historically, extensive spectroscopic investigations [3–12] have been carried out on the charge dynamics in poly(3-hexylthiophene) (P3HT)/[6, 6]-phenyl C_{61}-butyric acid methyl ester (PCBM) blend film, due to its reproducible power conservation efficiency (PCE > 5% [13, 14]). In particular, the regioregularity of P3HT, as well as the annealing process, has a significant effect on the charge dynamics of the P3HT/PCBM blend film [4, 7, 8]. Among them, Hwang et al. [4] investigated the charge dynamics in a regioregular-P3HT (RR-P3HT)/PCBM blend film and proposed a two-step process for charge generation, that is, formation of

the interfacial CT states (<250 fs) followed by the charge separation (=4 ps). We emphasize that their interpretation is based on the assignment of the photoinduced absorption (PIA) signals. They assigned the PIA at 1.7 eV to the donor polaron [15, 16], while they did that at 1.1–1.6 eV to the CT state. Unfortunately, the assignment of the PIAs of the RR-P3HT/PCBM blend film is still controversial. Another candidate of OPV is poly(9,9′-dioctylfluorene-co-bithiophene) (F8T2)/[6, 6]-phenyl C_{71}-butyric acid methyl ester ($PC_{70}BM$), because the fluorene-based copolymers, for example, F8T2, are more stable than the thiophene-based polymers, for example, P3HT. The solar cell using the blend film shows a PCE of 2.2–2.3% [17, 18].

In this study, we investigated the charge dynamics of two prototypical blend films, that is, RR-P3HT/PCBM and F8T2/$PC_{70}BM$ blend films. In order to assign the PIA signals, we decomposed differential absorption spectra into fast, slow, and constant components via two-exponential fittings at respective probe photon energies. The decomposition procedure clearly distinguished photoinduced absorptions (PIAs) due to D^*, CT, and D^+. We observed exciton conversion into the CT state ($D^* \rightarrow CT$) in both the blend films. The conversion speed (=0.7 ps) in the F8T2/$PC_{70}BM$ blend film is nearly the same as that (=1.2 ps) in the P3HT/PCBM blend film.

2. Experiment

2.1. Film Preparation for Optical Measurements. All materials (see Figure 1) were purchased from commercially available sources and used as received. F8T2 was purchased from American Dye Source. The weight average molecular weight (M_w), number average molecular weight (M_n), and polydispersity (M_w/M_n) were estimated to be 45000, 13000, and 3.4, respectively. RR-P3HT was purchased from Luminescence Technology Corp. The weight average molecular weight (M_w), number average molecular weight (M_n), and polydispersity (M_w/M_n) were estimated to be 44000, 22000, and 2.0, respectively. The fullerene derivatives, that is, PCBM and $PC_{70}BM$, were purchased from Solenne.

P3HT and P3HT/PCBM blend films were spin-coated on quartz substrates and annealed for 10 min at 110°C. Solutions of P3HT and that of blend with 50% PCBM by weight was prepared by dissolving the compounds in *o*-dichlorobenzene (20 mg polymer in 1 mL solution). The thickness of the P3HT and P3HT/PCBM blend films was 129 and 234 nm, respectively. F8T2 and F8T2/$PC_{70}BM$ blend films were spin-coated on quartz substrates and annealed for 10 min at 80°C. Solutions of F8T2 and that of blend with 66% $PC_{70}BM$ by weight were prepared by dissolving the compounds in *o*-dichlorobenzene (16 mg polymer in 1 mL solution). The thickness of the F8T2 and F8T2/$PC_{70}BM$ blend films was 87 and 89 nm, respectively. All the film preparation and post-treatment were performed in an inert N_2 atmosphere. The F8T2/$PC_{70}BM$ blend film shows a definite D/A interface [17, 19]. The average size of the $PC_{70}BM$ domains is 230 nm in diameter.

2.2. Preparation of OPV and Characterization. The F8T2/$PC_{70}BM$ OPV was fabricated in the following configuration: ITO/PEDOT: PSS (40 nm)/active layer/LiF (1.2 nm)/Al (80 nm). The patterned ITO (conductivity: 10 Ω/square) glass was precleaned in an ultrasonic bath of acetone and ethanol and then treated in an ultraviolet-ozone chamber. A thin layer (40 nm) of PEDOT: PSS was spin-coated onto the ITO and dried at 110°C for 10 min on a hot plate in air. The substrate was then transferred to an N_2 glove box and dried again at 110°C for 10 min on a hot plate. An *o*-dichlorobenzene solution of F8T2:$PC_{70}BM$ (1 : 2 by weight) was subsequently spin-coated onto the PEDOT:PSS surface to form the active layer. The resultant substrates were then annealed at 80°C for 10 min in an N_2 glove box. Finally, LiF (1.2 nm) and Al (80 nm) were deposited onto the active layer by conventional thermal evaporation at a chamber pressure lower than 5×10^{-4} Pa, which provided the devices with an active area of 2×2 mm^2. For comparison, we fabricated RR-P3HT/PCBM OPV in a similar procedure. An *o*-dichlorobenzene solution of RR-P3HT: PCBM (1 : 1 by weight) was subsequently spin-coated onto the PEDOT: PSS surface to form the active layer. The resultant substrates were then annealed at 110°C for 10 min in an N_2 glove box.

The current density-voltage (*J-V*) curves were measured using an ADCMT 6244 DC voltage current Source/Monitor under AM 1.5 solar-simulated light irradiation of 100 mWcm^{-2} (Wacom Electric Co., Ltd.). The incident photon-to-current conversion efficiency (IPCE) was measured using a CEP-2000 system (Bunkoh-Keiki Co., Ltd.).

2.3. Time-Resolved Spectroscopy. Ultrafast time-resolved spectroscopy was carried out in a pump-probe configuration at room temperature (Figure 2). We employed a regenerative amplified Ti: sapphire laser with a pulse width of 100 fs and a repetition rate of 1000 Hz as the light source. The pump pulse wavelength was 400 nm, which was generated as second harmonics in a β-BaB_2O_4 (BBO) crystal. The excitation intensity was 27–54 μJ/cm^2. The frequency of the pump pulse was decreased by half (500 Hz) to provide "pump-on" and "pump-off" condition. A white probe pulse (450–1600 nm), generated by self-phase modulation in a sapphire plate, was focused on the sample with the pump pulse. Spot sizes of the pump and probe pulses were 2.5 and 1.3 mm in diameter, respectively. The transmitted probe spectra were detected using a 72 ch Si photodiode array (450–900 nm) and/or a 256 ch InGaAs photodiode array (800–1600 nm) attached to a 30 cm imaging spectrometer. The spectral data were accumulated for 10000 pulses to improve the signal/noise ratio. The differential absorption spectra (ΔOD) are expressed as $\Delta OD = -\ln(I_{on}/I_{off})$, where I_{on} and I_{off} are the transmitted light intensity with and without pump excitation, respectively.

2.4. Optical Modulation Spectroscopy. Optical modulation spectroscopy was carried out in a pump-probe configuration at room temperature (Figure 3). A continuous wave Yttrium Aluminum Garnet (CW-YAG) laser (532 nm) was used as the excitation light source. The excitation intensity was

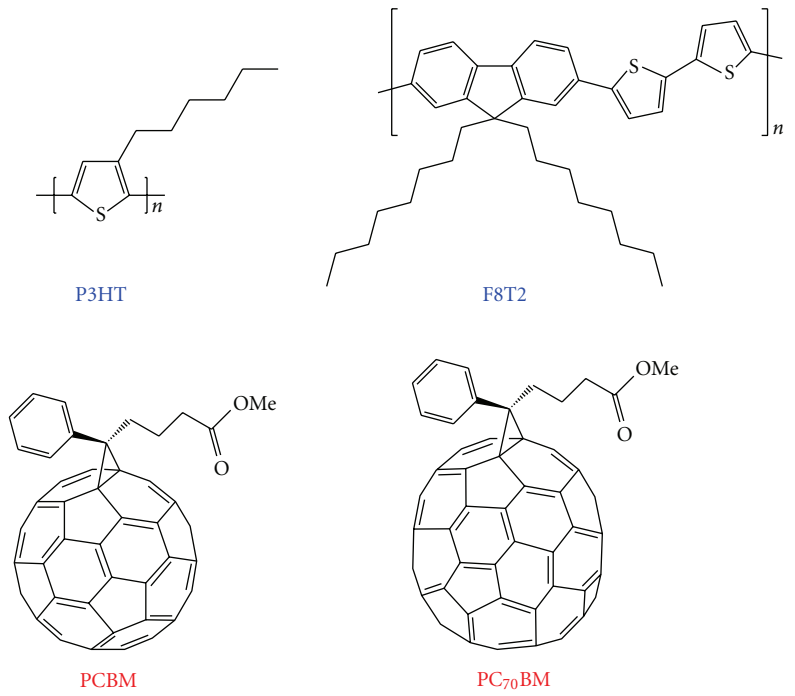

Figure 1: Molecular structures of poly(3-hexylthiophene) (P3HT), poly(9,9′-dioctylfluorene-co-bithiophene) (F8T2), [6, 6]-phenyl C_{61}-butyric acid methyl ester (PCBM), and [6, 6]-phenyl C_{71}-butyric acid methyl ester ($PC_{70}BM$).

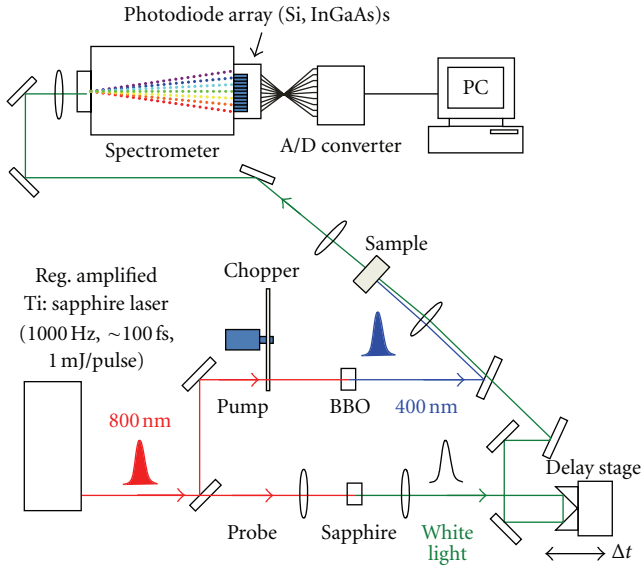

Figure 2: Schematic illustration of the experimental setup for time-resolved spectroscopy.

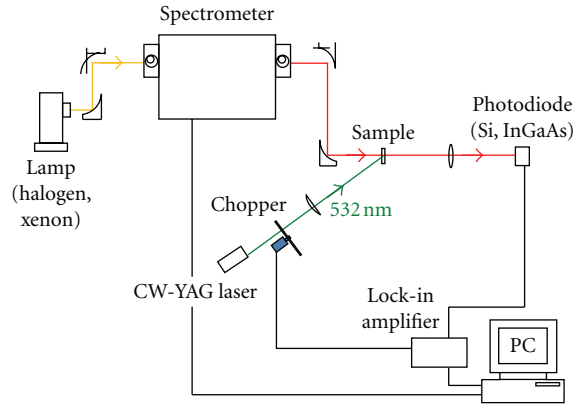

Figure 3: Schematic illustration of the experimental setup for optical modulation spectroscopy.

1.4 mW/cm^2, which was modulated with an optical chopper. The white light from the Halogen and/or Xe lamp was monochromatized with a 30 cm imaging spectrometer. The monochromatic probe light was focused on the sample with the pump light. The transmitted probe light was detected using a Si and/or InGaAs photodiode. A lock-in detection was adopted to extract the modulation signal. The optical modulation spectroscopy can clarify the PIA due to the long-lived D^+.

3. Results

3.1. OPV Properties of RR-P3HT/PCBM and F8T2/$PC_{70}BM$ Blend Films. Figure 4(a) shows current density-voltage (J-V) curves of OPVs based on the RR-P3HT/PCBM and F8T2/$PC_{70}BM$ blend films. The OPV based on F8T2 (HOMO of −5.46 eV) exhibits a high open-circuit voltage (V_{oc}) of 1.00 V, as compared with the value (=0.6 V) in typical OPVs based on RR-P3HT (HOMO of −4.70 eV). This is because V_{oc} is basically determined by the energy difference between D HOMO level and A LUMO (~−3.7 eV). The OPV based on the F8T2/$PC_{70}BM$ blend film exhibits a short circuit current (J_{sc}) of 4.28 mAcm^{-2}, a V_{oc} of 1.00 V, a fill factor (FF)

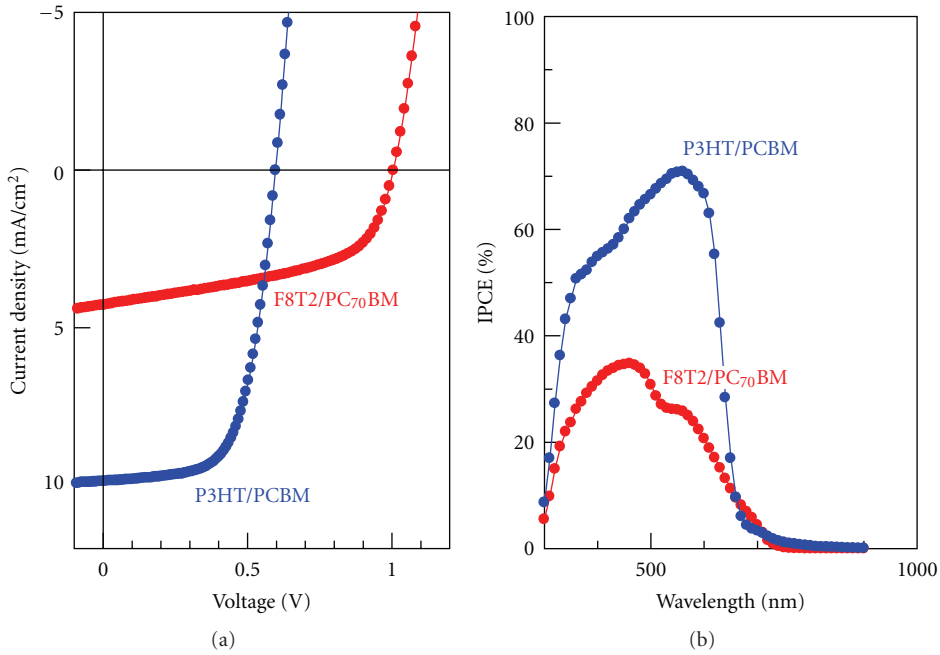

Figure 4: (a) J-V curves of OPVs based on the RR-P3HT/PCBM and F8T2/PC_{70}BM blend films. (b) IPCE spectra for OPVs based on the RR-P3HT/PCBM and F8T2/PC_{70}BM blend films.

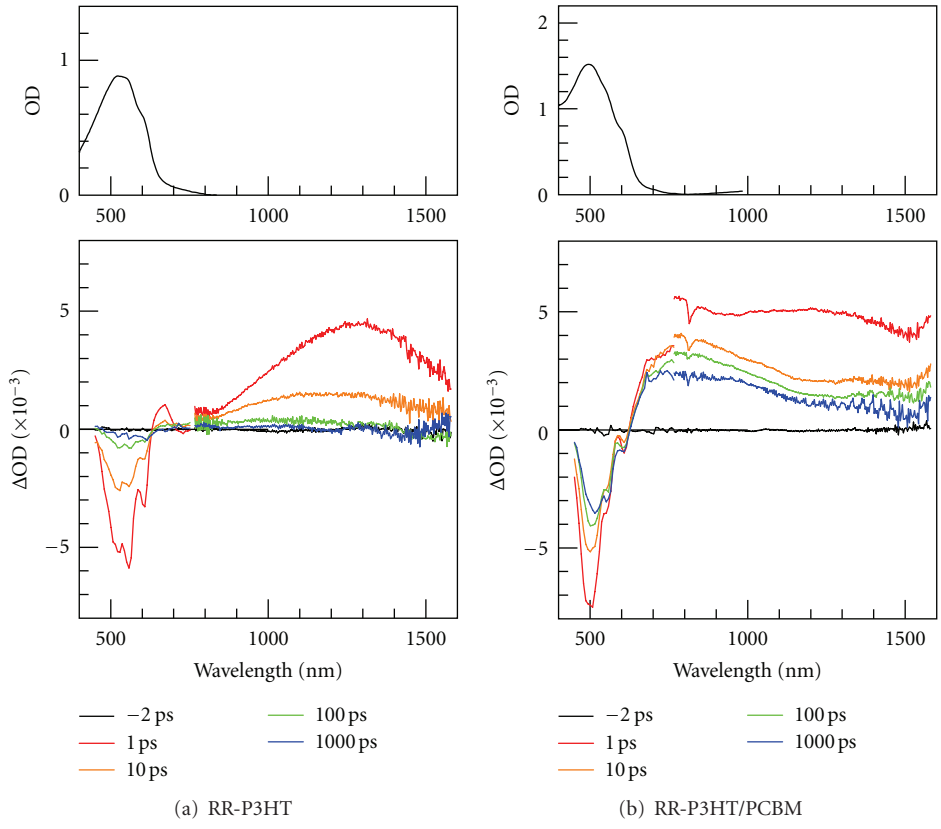

Figure 5: Absorption (OD) spectra and differential absorption (ΔOD) spectra of (a) neat RR-P3HT film and (b) RR-P3HT/PCBM blend films at 300 K.

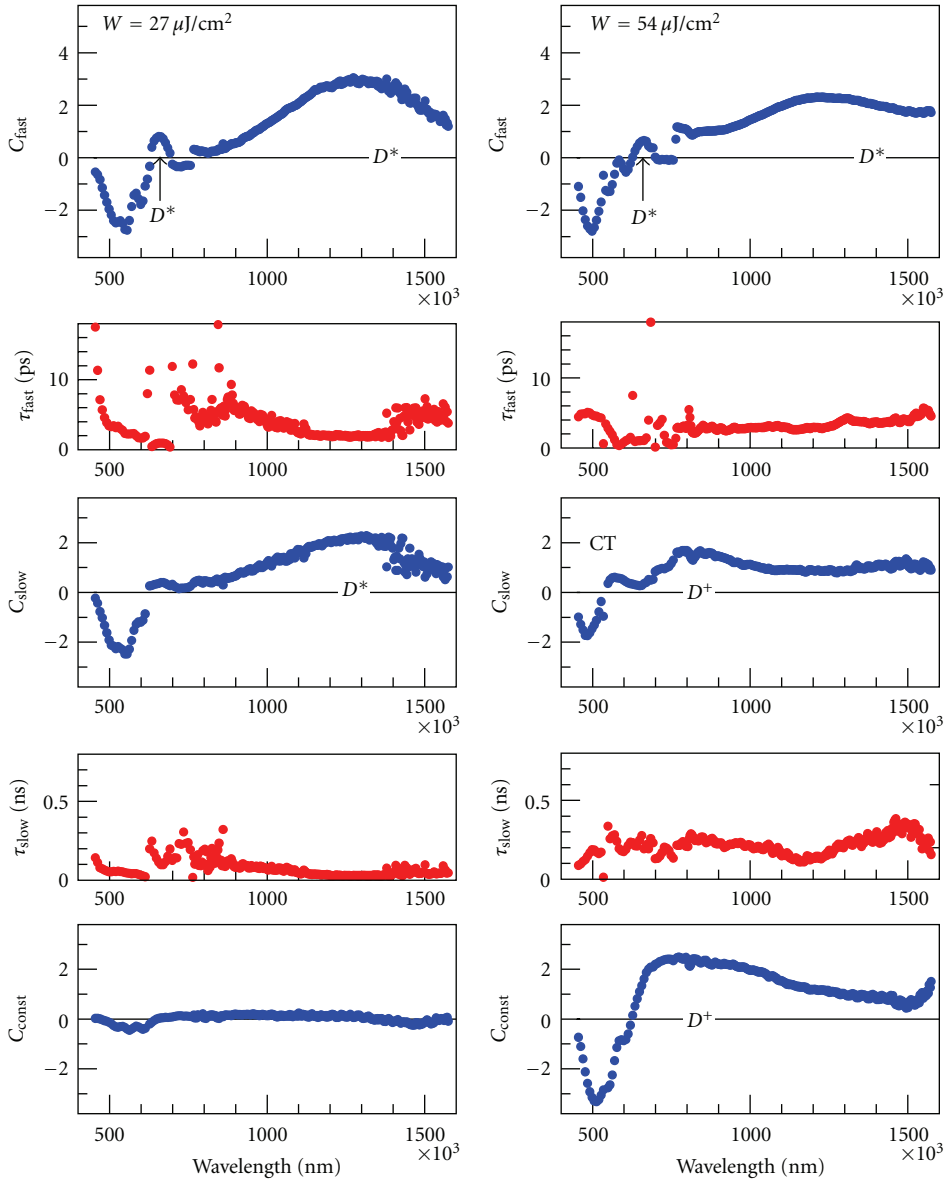

FIGURE 6: Decomposition of the time-resolved spectra of (a) neat RR-P3HT film and (b) RR-P3HT/PCBM blend films. The upper two panels are magnitudes (C_{fast}) and lifetimes (τ_{fast}) of the fast component. The middle two panels are magnitudes (C_{slow}) and lifetimes (τ_{slow}) of the slow component. The bottom panels are magnitudes (C_{const}) of the constant component. D*, CT, and D$^+$ represent PIAs due to singlet exciton, CT state, and carrier, respectively.

of 0.53, and a PCE of 2.28%. The OPV based on the RR-P3HT/PCBM blend film exhibits a J_{sc} of 9.9 mAcm^{-2}, a V_{oc} of 0.60 V, a, FF of 0.64, and a PCE of 3.8%.

Figure 4(b) shows wavelength dependence of the photovoltaic response for the OPVs based on the RR-P3HT/PCBM and F8T2/PCBM blend films. In all the wavelength region, the IPCE values for the F8T2/PCBM blend film are smaller than those for the RR-P3HT/PCBM blend film. The IPCE values at 400 nm are 54% and 30% for the RR-P3HT/PCBM and F8T2/PCBM blend films, respectively.

3.2. Time-Resolved Spectra of RR-P3HT and RR-P3HT/PCBM Films. Figure 5 shows ΔOD spectra (lower panels) of (a) neat RR-P3HT film and (b) RR-P3HT/PCBM blend films, together with their linear absorption spectra (OD: upper panels). As seen in the OD spectra, the pump pulse (at 400 nm) efficiently excites the D polymer. In all the films, the ΔOD spectra consist of negative signals in the short-wavelength region and positive signals in the long-wavelength region. The negative signal is ascribed to the ground state bleach (GSB) as well as the stimulated emission (SE) of singlet exciton luminescence. On the other hand, the positive signal is ascribed to PIAs due to the photogenerated species, such as D*, CT, and D$^+$.

Generally speaking, the lifetime is a good physical quantity that distinguishes the PIAs due to different excited

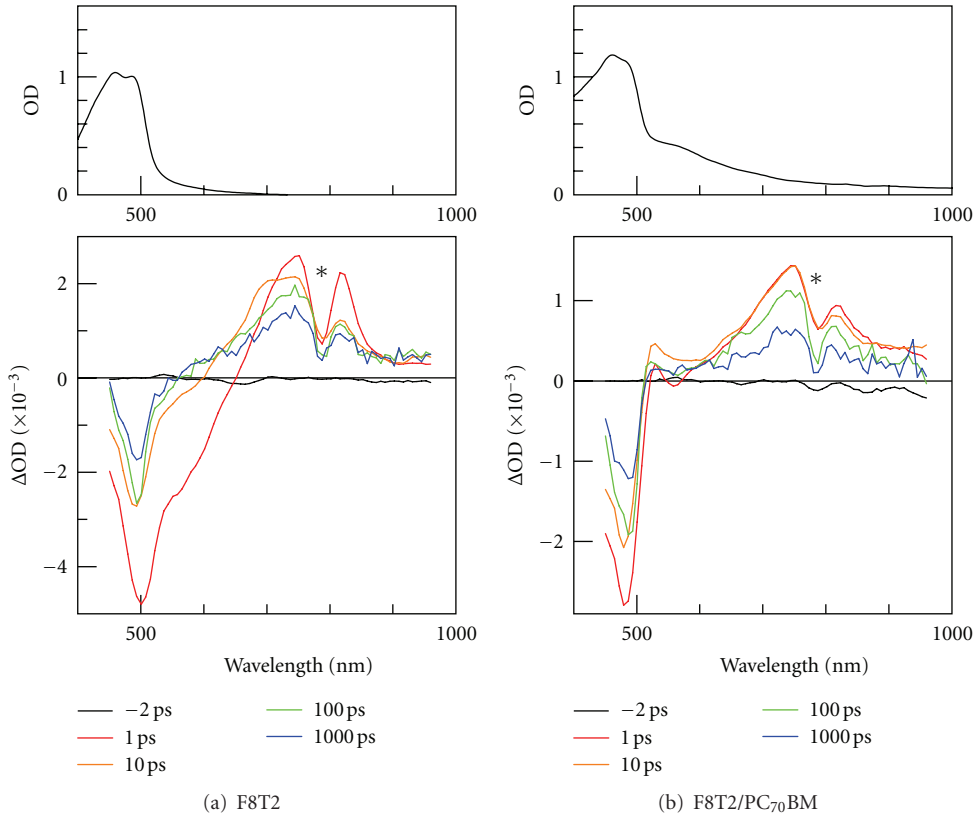

FIGURE 7: Absorption (OD) spectra and differential absorption (ΔOD) spectra of (a) neat F8T2 film and (b) F8T2/$PC_{70}BM$ blend films at 300 K. Star symbols indicate an artificial structure due to the notch filter at 800 nm.

species: for example, lifetime of D^* is much faster than that of D^+. In order to decompose the time-resolved spectra into fast, slow and constant components, we analyzed the decay curve at respective probe photon energies with two exponential functions:

$$\Delta\mathrm{OD} = C_{\mathrm{fast}} \times \exp\left(-\frac{t}{\tau_{\mathrm{fast}}}\right) + C_{\mathrm{slow}} \times \exp\left(-\frac{t}{\tau_{\mathrm{slow}}}\right) + C_{\mathrm{const}}, \quad (1)$$

where C_{fast} (τ_{fast}), C_{slow}(τ_{slow}), and C_{const} are the magnitude (lifetime) of the respective components [20]. Thus obtained parameters, C_{fast}, τ_{fast}, C_{slow}, τ_{slow}, and C_{const} are plotted in Figure 6 against wavelength.

Figure 6(a) shows the spectral components of the neat P3HT film. In the C_{fast} component, a negative peak around 550 nm is ascribed to the GSB and SE. On the other hand, a positive sharp signal at 650 nm and broad signal at ~1300 nm are ascribed to the PIA due to D^*. In the C_{slow} component, the broad PIA due to D^* is discernible at ~1300 nm. No signal is observed in the C_{slow} component.

Figure 6(b) shows the spectral components of the RR-P3HT/PCBM blend film. In the C_{fast} component, the spectral profile is almost the same as the neat RR-P3HT film: negative signal due to GSB and SE at 500 nm and PIAs due to D^* at 650 nm and ~1300 nm. In the C_{slow} component, the PIA due to D^* completely disappears and new PIAs appears at 570 nm and ~800 nm. In the C_{const} component, broad PIA at ~700 nm is observed. Jiang et al. [16] performed optical modulation spectroscopy in the neat RR-P3HT film and observed polaron signals at ~670 nm and ~1000 nm. They ascribed the former and latter signals to the free and localized carriers, respectively. According to their assignments, we ascribed the PIAs at ~700 nm (C_{const}) and at ~800 nm (C_{slow}) to the free and localized carriers, respectively. Based on the assignments of PIAs in the F8T2/$PC_{70}BM$ blend film, we ascribed the PIA at 570 nm (C_{slow}) to the CT state (*vide infra*).

3.3. Time-Resolved Spectra of F8T2 and F8T2/$PC_{70}BM$ Films. Figure 7 shows ΔOD spectra (lower panels) of (a) neat F8T2 film and (b) F8T2/$PC_{70}BM$ blend films, together with the OD spectra (upper panels). As seen in the OD spectra, the pump pulse (at 400 nm) efficiently excites the D polymer. In all the films, the ΔOD spectra consist of negative signals in the short-wavelength region and positive signals in the long-wavelength region. The negative signal is ascribed to GSB and/or SE. On the other hand, the positive signal is ascribed to PIAs due to the photo-generated species, such as D^*, CT, and D^+. We analyzed the decay curve at respective probe photon energies with two exponential functions (1). Obtained parameters C_{fast}, τ_{fast}, C_{slow}, τ_{slow}, and C_{const} are plotted in Figure 8 against wavelength.

Figure 8(a) shows the spectral components of the neat F8T2 film. In the C_{fast} component, a negative peak at 506 nm are ascribed to the GSB, whereas a negative peak at 553 nm

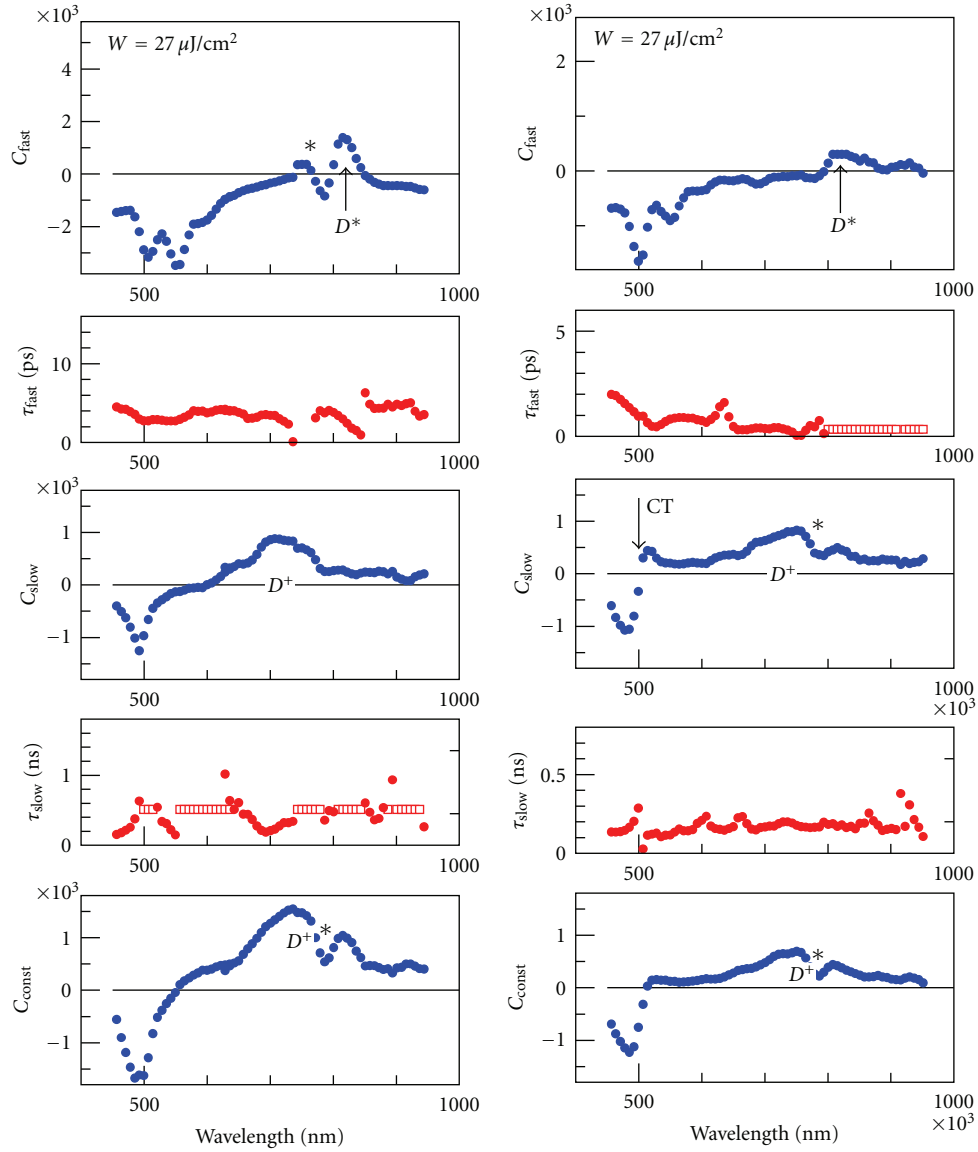

Figure 8: Decomposition of the time-resolved spectra of (a) neat F8T2 film and (b) F8T2/$PC_{70}BM$ blend films. The upper two panels are magnitudes (C_{fast}) and lifetimes (τ_{fast}) of the fast component. The middle two panels are magnitudes (C_{slow}) and lifetimes (τ_{slow}) of the slow component. The bottom panels are magnitudes (C_{const}) of the constant component. Open symbols indicate that the parameter is fixed in the fitting procedure. Star symbols indicate artificial structures due to the notch filter at 800 nm. D*, CT, and D^+ represent PIAs due to singlet exciton, CT state, and carrier, respectively.

and the broad background extending from 500 to 700 nm is ascribed to the SE. Actually, the luminescence spectra of the F8T2 film extend from 500 to 700 nm with a peak at 550 nm. [21] On the other hand, a positive sharp signal around 800 nm is ascribed to the PIA due to D*. Actually, the exciton lifetime (=2.7 ps) is comparable to the decay time (~3 ps) of the SE signal. In the C_{slow} component, a positive broad signal is observed at ~700 nm. We ascribed the signal to the PIA due to D^+, because a long-lived polaron signal was observed at ~800 nm in the optical modulation spectrum of the F8T2/$PC_{70}BM$ blend film (see Figure 9).

Figure 8(b) shows the spectral component of the F8T2/$PC_{70}BM$ blend film. In the C_{fast} component, the GSB signal is observed at 501 nm, whereas the SE signal (500–700 nm) is rather suppressed. The suppression of the SE signal is probably due to the doping-induced luminescence quenching [21]. The PIA due to D* is discernible at 800 nm. In the C_{slow} component, the PIA due to D* completely disappears and new PIAs appears at 520 nm and ~700 nm. The PIA at ~700 nm is due to D^+, because a long-lived carrier'signal was observed at ~800 nm in the optical modulation spectrum of the F8T2/$PC_{70}BM$ blend film (see Figure 9). For the following reason, we ascribed the 520 nm signal to the PIA

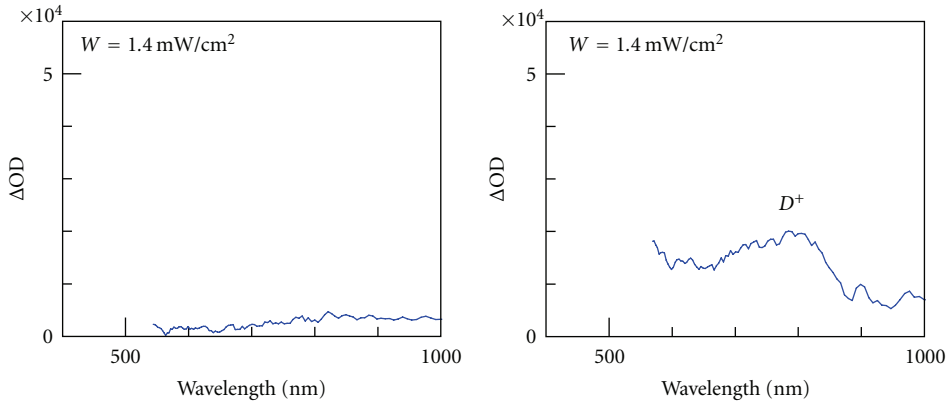

Figure 9: Optical modulation spectra of (a) neat F8T2 film and (b) F8T2/$PC_{70}BM$ blend films.

due to the CT state. We compared the C_{slow} component in the 1 : 3 blend film (not shown) with that of the 1 : 2 film [19]. The average size of the $PC_{70}BM$ domains is 300 nm (230 nm) in diameter in the 1:3 (1 : 2) blend film: the interface region is much reduced in the 1 : 3 film. We found that the 520 nm signal is suppressed in the 1 : 3 film, suggesting that the 520 nm signal relates to the interface. In addition, Lim et al. [21] reported an extra 570 nm absorption in the F8T2 film, in which 8% 2,3,5,6-tetrafluoro-7,7,8,8-tetracyanoquinodimethane (F_4TCNQ) is doped as an oxidant. They ascribed the 570 nm absorption to a CT complex, that is, $F8T2^+$-F_4TCNQ^-. Analogously, the CT state, that is, $F8T2^+$-$PC_{70}BM^-$, in our blend film is responsible for the PIA at 520 nm. In the C_{slow} component, PIA due to the CT state disappears, and only the PIA due to D^+ is observed.

Here, we note that the energy position and temporal behavior of the PIA at 570 nm in the RR-P3HT/PCBM blend film are analogues to the PIA at 570 nm in the F8T2/$PC_{70}BM$ blend film. This strongly suggests that the PIA at 570 nm in the F8T2/$PC_{70}BM$ blend film is also ascribed to the CT state.

3.4. Optical Modulation Spectra of F8T2 and F8T2/$PC_{70}BM$ Films. Figure 9 shows optical modulation spectra of (a) F8T2 and (b) F8T2/$PC_{70}BM$ blend films. No signal is observed in the neat F8T2 film. In the F8T2/$PC_{70}BM$ blend film, characteristic positive signal is observed at ∼800 nm due to the long-lived carriers. Consistently, Ravirajan et al. [22] re-ported positive polaron signal at 720 nm in the chemically oxidized F8T2.

4. Discussions

Figure 10 shows temporal evolution of the PIAs of RR-P3HT/PCBM blend film due to D*, CT state, and D^+. Solid curves are the results of least-squares fitting with (1). The exciton lifetime (τ_{fast} = 0.9 ps) is close to the formation time (τ_{fast} = 1.2 ps) of the CT state, indicating exciton conversion into the CT state (D* → CT). The finite rise time of the CT state suggests that the state is created by exciton conversion at the interface, rather than by direct photo-generation. On the other hand, the PIA due to D^+ exhibits a monotonic decrease with time, implying that D^+ is created mainly by direct photogeneration, not by conversion from the CT state. The number of D^+ gradually decreases and becomes 65% of the initial state at ∼1 ns. Note that the apparent constant component of 660 nm and at 560 nm should be ascribed to the broad PIA due to D^+ and GSB, respectively.

Figure 11 shows temporal evolution of the PIAs of F8T2/$PC_{70}BM$ blend film due to D*, CT state, and D^+. Solid curves are the results of least-squares fitting with (1). The exciton lifetime (τ_{fast} = 2.0 ps) is close to the formation time (τ_{fast} = 0.7 ps) of the CT state, indicating exciton conversion into the CT state (D* → CT). The finite rise time of the CT state suggests that the state is created by exciton conversion at the interface, rather than by direct photo-generation. On the other hand, the PIA due to D^+ exhibits a monotonic decrease with time, implying that D^+ is created mainly by direct photo-generation, not by conversion from the CT state. The number of D^+ gradually decreases and becomes 40% of the initial state at ∼1 ns. Note that the apparent constant component of 800 nm should be ascribed to the broad PIA due to D^+.

Finally, let us comment on the plasmonic enhancement effect, which is a key technique to design the highly efficient OPV. For example, Poh et al. [23] clearly demonstrated that gold nanoparticles on the PEDOT-PSS enhance the PCE of the bilayer P3HT-C_{60} device. They ascribed the enhancement to the enhanced absorption based on a finite-difference time-domain method (FDTD) simulation. We suspect that existence of the metal nanoparticle significantly influences the charge formation dynamics itself via the strong local field around the metal nanoparticles, especially when they locate near the D-A interface. We emphasize that the ultrafast spectroscopy is a powerful tool to clarify the plasmonic effects on the charge formation dynamics.

5. Summary

We investigated the charge dynamics of two prototypical blend films, that is, RR-P3HT/PCBM and F8T2/$PC_{70}BM$

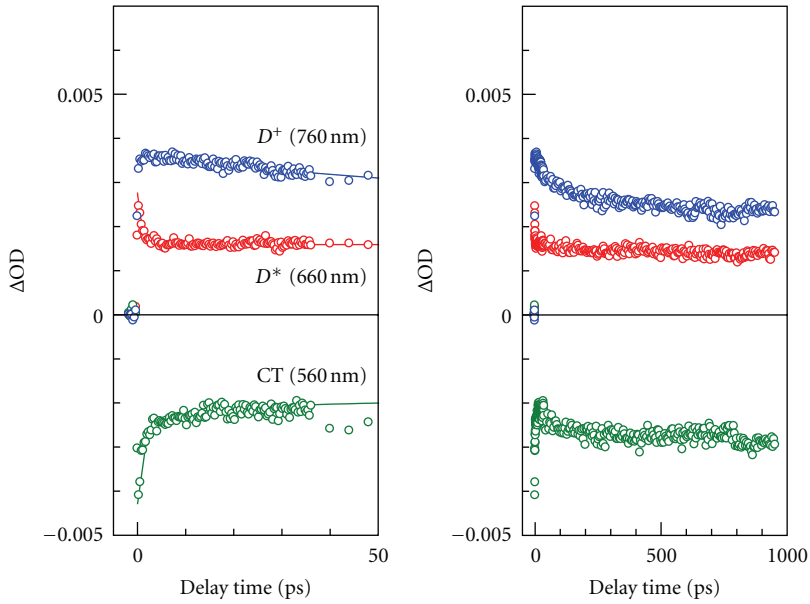

(a) RR-P3HT/PCBM (b) RR-P3HT/PCBM

FIGURE 10: Temporal evolutions of PIAs of RR-P3HT/PCBM blend film due to D*, CT state, and D+: (a) fast region and (b) slow region. Solid curves in (a) are results of least-squares fitting with exponential functions: $\Delta OD = C_{fast} \times \exp(-t/\tau_{fast}) + C_{slow} \times \exp(-t/\tau_{slow}) + C_{const}$, C_{fast} is fixed at 0 in the PIA due to D^+.

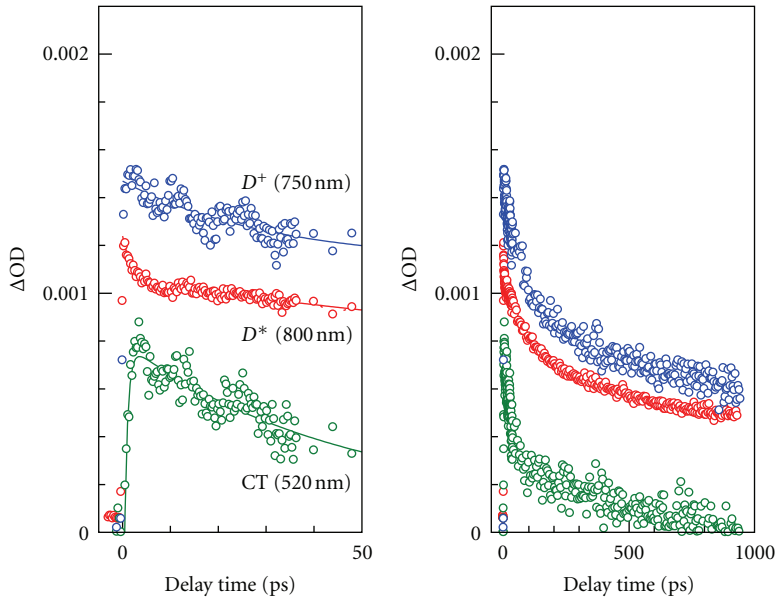

(a) F8T2/PC_{70}BM (b) F8T2/PC_{70}BM

FIGURE 11: Temporal evolutions of PIAs of F8T2/PC_{70}BM blend film due to D*, CT state, and D+: (a) fast region and (b) slow region. Solid curves in (a) are results of least-squares fitting with exponential functions: $\Delta OD = C_{fast} \times \exp(-t/\tau_{fast}) + C_{slow} \times \exp(-t/\tau_{slow}) + C_{const}$, C_{fast} is fixed at 0 in the PIA due to D^+.

blend films. We observed exciton conversion into the CT state ($D^* \rightarrow CT$) in both the blend films. The conversion speed (=0.7 ps) in the F8T2/PC_{70}BM blend film is nearly the same as that (=1.2 ps) in the P3HT/PCBM blend film. Most of the carriers, however, are created by direct photogeneration, not by conversion from the CT state. The number of D^+ gradually decreases to 65% (40%) of the initial state at ~1 ns in the RR-P3HT/PCBM (F8T2/PC_{70}BM) blend film. The faster recombination ratio perhaps causes the lower PCE in the F8T2/PC_{70}BM blend film.

Acknowledgment

This work was supported by a Grant-in-Aid for Young Scientists (B) (22750176) for Scientific Research from the Ministry of Education, Culture, Sports, Science and Technology, Japan.

References

[1] M. Hiramoto, H. Fujiwara, and M. Yokoyama, "Three-layered organic solar cell with a photoactive interlayer of codeposited pigments," *Applied Physics Letters*, vol. 58, no. 10, pp. 1062–1064, 1991.

[2] N. S. Sariciftci, L. Smilowitz, A. J. Heeger, and F. Wudl, "Photoinduced electron transfer from a conducting polymer to buckminsterfullerene," *Science*, vol. 258, no. 5087, pp. 1474–1476, 1992.

[3] G. Grancini, D. Polli, D. Fazzi, J. Cabanillas-Gonzalez, G. Cerullo, and G. Lanzani, "Transient absorption imaging of P3HT:PCBM photovoltaic blend: evidence for interfacial charge transfer state," *Journal of Physical Chemistry Letters*, vol. 2, no. 9, pp. 1099–1105, 2011.

[4] I.-W. Hwang, D. Moses, and A. J. Heeger, "Photoinduced carrier generation in P3HT/PCBM bulk heterojunction materials," *Journal of Physical Chemistry C*, vol. 112, no. 11, pp. 4350–4354, 2008.

[5] S. Trotzky, T. Hoyer, W. Tuszynski, C. Lienau, and J. Parisi, "Femtosecond up-conversion technique for probing the charge transfer in a P3HT : PPCBM blend via photoluminescence quenching," *Journal of Physics D*, vol. 42, no. 5, Article ID 055105, 2009.

[6] J. Guo, H. Ohkita, H. Benten, and S. Ito, "Near-IR femtosecond transient absorption spectroscopy of ultrafast polaron and triplet exciton formation in polythiophene films with different regioregularities," *Journal of the American Chemical Society*, vol. 131, no. 46, pp. 16869–16880, 2009.

[7] J. Guo, H. Ohkita, H. Benten, and S. Ito, "Charge generation and recombination dynamics in poly(3-hexylthiophene)/fullerene blend films with different regioregularities and morphologies," *Journal of the American Chemical Society*, vol. 132, no. 17, pp. 6154–6164, 2010.

[8] R. Alex Marsh, J. M. Hodgkiss, S. Albert-Seifried, and R. H. Friend, "Effect of annealing on P3HT:PCBM charge transfer and nanoscale morphology probed by ultrafast spectroscopy," *Nano Letters*, vol. 10, no. 3, pp. 923–930, 2010.

[9] J. Piris, T. E. Dykstra, A. A. Bakulin et al., "Photogeneration and ultrafast dynamics of excitons and charges in P3HT/PCBM blends," *Journal of Physical Chemistry C*, vol. 113, no. 32, pp. 14500–14506, 2009.

[10] I. A. Howard, R. Mauer, M. Meister, and F. Laquai, "Effect of morphology on ultrafast free carrier generation in polythiophene: fullerene organic solar cells," *Journal of the American Chemical Society*, vol. 132, no. 42, pp. 14866–14876, 2010.

[11] S. Cook, R. Katoh, and A. Furube, "Ultrafast studies of charge generation in PCBM: P3HT blend films following excitation of the fullerene PCBM," *Journal of Physical Chemistry C*, vol. 113, no. 6, pp. 2547–2552, 2009.

[12] S. Cook, A. Furube, and R. Katoh, "Analysis of the excited states of regioregular polythiophene P3HT," *Energy and Environmental Science*, vol. 1, no. 2, pp. 294–299, 2008.

[13] W. Ma, C. Yang, X. Gong, K. Lee, and A. J. Heeger, "Thermally stable, efficient polymer solar cells with nanoscale control of the interpenetrating network morphology," *Advanced Functional Materials*, vol. 15, no. 10, pp. 1617–1622, 2005.

[14] Y. Kim, S. Cook, S. M. Tuladhar et al., "A strong regioregularity effect in self-organizing conjugated polymer films and high-efficiency polythiophene:fullerene solar cells," *Nature Materials*, vol. 5, no. 3, pp. 197–203, 2006.

[15] O. J. Korovyanko, R. Osterbacka, X. M. Jiang, and Z. V. Vardeny, "Theory of the electronic structure of the alloys of the actinides," *Physical Review B*, vol. 64, no. 23, Article ID 235122, 10 pages, 2001.

[16] X. M. Jiang, R. Osterbacka, O. Korovyanko et al., "Spectroscopic studies of photoexcitations in regioregular and regiorandom polythiophene films," *Advanced Functional Materials*, vol. 12, no. 9, pp. 587–597, 2002.

[17] T. Yasuda, K. Yonezawa, M. Ito, H. Kamioka, L. Han, and Y. Moritomo, "Photovoltaic properties and charge dynamics in nanophase-separated F8T2/PCBM blend films," *Journal of Photopolymer Science and Technology*. In press.

[18] J.-H. Huang, C.-P. Lee, Z.-Y. Ho, D. Kekuda, C.-W. Chu, and K.-C. Ho, "Enhanced spectral response in polymer bulk heterojunction solar cells by using active materials with complementary spectra," *Solar Energy Materials and Solar Cells*, vol. 94, no. 1, pp. 22–28, 2010.

[19] K. Yonezawa, H. Kamioka, T. Yasuda, L. Han, and Y. Moritomo, "Charge-transfer state and charge dynamics in poly(9, 9-dioctylfluorene-co-bithiophene) and [6, 6]-phenyl C_{70}-butyric acid methyl ester blend film," *Applied Physics Express*, vol. 4, no. 12, Article ID 122601, 2011.

[20] H. Kamioka, Y. Moritomo, W. Kosaka, and S. Ohkoshi, "Charge-transfer dynamics in cyano-bridged M_A–Fe system (M_A = Mn, Fe, and Co)," *Journal of the Physical Society of Japan*, vol. 77, no. 9, Article ID 093710, 2008.

[21] R. Lim, B.-J. Jung, M. Chikamatsu et al., "Doping effect of solution-processed thin-film transistors based on polyfluorene," *Journal of Materials Chemistry*, vol. 17, no. 14, pp. 1416–1420, 2007.

[22] P. Ravirajan, S. A. Haque, D. Poplavskyy, J. R. Durrant, D. D. C. Bradley, and J. Nelson, "Nanoporous TiO_2 solar cells sensitised with a fluorene-thiophene copolymer," *Thin Solid Films*, vol. 451-452, pp. 624–629, 2004.

[23] C. H. Poh, L. Rosa, S. Juodkazis, and P. Dastoor, "FDTD modeling to enhance the performance of an organic solar cell embedded with gold nanoparticle," *Optical Materials Express*, vol. 1, pp. 1326–1331, 2011.